Tissue Morphology and Gene Expression Characterisation of Transplantable Adenocarcinoma Bearing Mice Exposed to Fluorodeoxyglucose-Conjugated Magnetic Nanoparticles

Adam J. Watkins[1,*], Gillian Pearce[2], Perihan Unak[3], Ozge K. Guldu[3], Volkan Yasakci[3], Oguz Akin[4], Omer Aras[4], Julian Wong[5], and Xianghong Ma[2]

[1] *Aston Research Centre for Healthy Ageing, School of Life and Health Sciences, Aston University, Birmingham, B4 7ET, United Kingdom*
[2] *School of Engineering and Applied Sciences, Aston University, Birmingham, B4 7ET, United Kingdom*
[3] *Ege University, Institute of Nuclear Sciences, Department of Nuclear Applications, 35100, Turkey*
[4] *Memorial Sloan Kettering Cancer Center, Department of Radiology, 1275 York Avenue, New York, NY 10065, USA*
[5] *Division of Vascular & Endovascular Surgery, Department of Cardiac, Thoracic & Vascular Surgery, National University Heart Centre, Singapore, 119228, Singapore*

Fluorodeoxyglucose-conjugated magnetic nanoparticles, designed to target cancer cells with high specificity when heated by an alternating magnetic field, could provide a low-cost, non-toxic treatment for cancer. However, it is essential that the *in vivo* impacts of such technologies on both tumour and healthy tissues are characterised fully. Profiling tissue gene expression by semi-quantitative reverse transcriptase real-time PCR can provide a sensitive measurement of tissue response to treatment. However, the accuracy of such analyses is dependent on the selection of stable reference genes. In this study, we determined the impact of fluorodeoxyglucose-conjugated magnetic nanoparticles on tumour and non-tumour tissue gene expression and morphology in MAC16 adenocarcinoma established male NMRI mice. Mice received an injection of 8 mg/kg body weight fluorodeoxyglucose-conjugated magnetic nanoparticles either intravenously in to the tail vein, directly into the tumour or subcutaneously directly overlying the tumour. Tissues from mice were sampled between 70 minutes and 12 hours post injection. Using the bioinformatic geNorm tool, we established the stability of six candidate reference genes (*Hprt*, *Pgk1*, *Ppib*, *Sdha*, *Tbp* and *Tuba*); we observed *Pgk1* and *Ppib* to be the most stable. We then characterised the expression profiles of several apoptosis genes of interest in our adenocarcinoma samples, observing differential expression in response to mode of administration and exposure duration. Using histological assessment and fluorescent TUNNEL staining, we observed no detrimental impact on either tumour or non-tumour tissue morphology or levels of apoptosis. These observations define the underlying efficacy of fluorodeoxyglucose-conjugated magnetic nanoparticles on tumour and non-tumour tissue morphology and gene expression, setting the basis for future studies.

KEYWORDS: Apoptosis, Gene Expression, Reference Gene, Magnetic Nanoparticles, Adenocarcinoma Mouse Model.

INTRODUCTION

Despite decades of research and significant financial investment, a definitive treatment or cure for cancer remains elusive. Current treatments including surgery, radiotherapy and chemotherapy are associated with detrimental side-effects and adverse impacts on patient appearance, well-being and health.[1] In addition, cancer cells can be inaccessible to treatment options such as surgery, can develop resistance to chemotherapeutic agents used in the treatment of cancer or remain incurable with current radiotherapy and chemotherapy approaches.[2,3] Finally, there are significant limitations for identifying and targeting individual cancer cells within patients, thereby limiting the delivery of treatment and

appropriate monitoring of treatment responses. As such, there is clear potential for the development and implementation of new approaches for the treatment of cancer.

One such approach is though the synthesis and surface modification of magnetic nanoparticles (MNPs). Studies have largely focused on the use of iron oxide containing MNPs on account of their biocompatibility and low toxicity.[4–6] However, in recent years, the synthesis of MNPs has improved substantially, resulting in the development of particles with specific surface coatings such as dextran,[7] polyethylene glycol,[8] gold[9] and dopamine.[10] The use of MNPs has been shown to result in many therapeutic benefits.[11–13] Moreover, they have low aggregation properties, enabling then to avoid emboli, are able to be incorporated easily into drug delivery systems and can be heated directly within an alternating magnetic field.[14–17] In addition, the use of magnetic field stimulation to induce tumour cell hyperthermia following intravenous administration of MNPs has been shown to be beneficial in controlling tumour growth.[18–21] Recently, we tested the *in vitro* functionality of fludeoxyglucose-conjugated magnetic nanoparticles (FDG-MNPs) with the aim of targeting MCF-7 cancer cells *in vitro* by magnetic field stimulation. As cancer cells are characterised by increased glycolysis and elevated lactate production,[22, 23] a phenomenon known as the Warburg effect,[24] their higher metabolic status results in preferential uptake of FDG-MNPs over non-cancerous cells. We observed rapid and sustained hyperthermia, resulting in the death of 89% of MCF-7 cancer cells *in vitro*.[25]

While these studies demonstrate the validity of using FDG-MNPs to target cancer cells *in vitro*, it is essential that their impact on non-cancerous tissue *in vivo* is established. Currently, morphological and gene expression analysis of tissues can be undertaken to understand cellular responses that may occur prior to observing changes at the histological level. Central to the measurement of gene expression profiles is the use of semi-quantitative reverse transcription real-time PCR (RT-qPCR).[25] This technique is both sensitive enough to detect changes in gene expression at single cell resolution[26] and robust enough to validate genome-wide expression analyses such as microarray data. However, in order to determine the expression levels of any gene of interest, its expression must be normalised against that of a reference gene.[27] Such reference genes must display stable expression profiles as they need to account for the multiple processing steps that take place during tissue isolation, cDNA synthesis, plate set up and PCR as well as for differences in target gene expression.[28] Interestingly, studies have shown that the expression of commonly used reference genes change with age,[30, 31] experimental conditions[32] and species.[33, 34] In addition, studies are now also defining appropriate reference gene selection within tumour tissue and cancer cell lines.[35–37]

Therefore, the aim of the present study was to define the impact of our FDG-MNPs in their non-magnetic stimulated state on tumour and non-tumour tissue in mice bearing MAC16 adenocarcinomas in a non-magnetic field environment. Here, we establish the expression profile of commonly used reference genes in a mouse adenocarcinoma model exposed to FDG-MNPs. Following selection of the most stable reference genes, we profiled the expression of several pro-apoptotic (*Bad*, *Bax*, *Casp1*, *Fas*) and anti-apoptotic genes (*Bcl2*, *cl2l1*) within the same tumour tissue samples. Finally, we demonstrate that *in vivo* administration of FDG-MNPs, in their non-magnetic stimulated state, has minimal impact on tumour and non-tumour tissue integrity or levels of cell death. However, we do observe large variances in reference gene expression profiles, highlighting the necessity to select appropriate reference genes in the analysis of tumour gene expression.

MATERIALS AND METHODS
Synthesis of Magnetic Nanoparticles (MNPs)

MNPs were prepared as previously described.[25] Briefly, 12 mL of 2 M $FeCl_3$ (Fluka, Istanbul, Turkey) solution in 2 M HCl (Merck, Istanbul, Turkey) was added to a 500 mL three necked glass flask. 50 mL of a freshly prepared 80 mM Na_2SO_3 (Merck) solution followed by 5 ml of NH_3 solution (25%) (Merck) added to the flask, both dropwise under nitrogen gas. The solution was incubated for 30 minutes at 70 °C and then cooled to below 45 °C. The black precipitate was recovered using an external magnetic field and washed with distilled water several times. Particles were then washed with a water–ethanol (2:1) mixture and the precipitate was re-suspended in 80% ethanol (Merck) prior to the addition of tetraethyl orthosilicate (TEOS, Sigma). The resulting solution was incubated for 12 hours at 40 °C. After 12 hours, silica-coated magnetic nanoparticles were washed with methanol and re-dispersed in 100 mL methanol. Using the Malvern Zetasizer Nano ZS (Malvern, Herrenberg, Germany), the mean hydrodynamic radius of the MNPs was 19.43 ± 2.30 nm.

Modification of Silica Coated Magnetite Nanoparticles with Amino-Silane

Silica-coated MNPs were mixed with 2.5 mL of (3-aminopropyl) triethoxysilane (APTES, Sigma) and placed within an ultrasonic water bath prior to being incubated for 12 hours at 60 °C with rapid stirring. The resulting MNPs were washed with ethanol prior to analysis of hydrodynamic radius (Malvern Zetasizer Nano ZS (Malvern, Herrenberg, Germany) which was 6.19 ± 1.85 nm.

Synthesis of NaF Substituted Mannose Triflate-Cysteamine

FDG-MNPs were prepared as described previously.[25] Briefly, for the synthesis of mannose triflate-cysteamine,

19.21 mg of mannose triflate (Fluka) was dissolved in 200 μL of distilled water at 90 °C. Separately, 84.85 mg of cysteamine (2-aminoetanethiol; Sigma, Istanbul, Turkey) was dissolved in 70 μL of pure water and adjusted to a pH of 7.5 prior to the addition of 40 mg of NaCNBH$_3$ (Fluka). Both solutions were mixed and heated for 1 hour at 90 °C prior to being precipitated, dried overnight at 65 °C and dissolved in dimethyl formamide (Merck). Next, 100 μL of Kryptofix (Merck) solution (2.0 mg/mL in dimethyl formamide), 200 μL of K$_2$CO$_3$ (Fluka) aqueous solution (2.0 mg/mL), 100 μL of dimethyl formamide (Merck) and 200 μL of 16 mM NaF (Merck) were added to 1 ml of the prepared mannose triflate-cysteamine (35 mM) and heated for 20 minutes at 90 °C in a water bath. For purification, the product was passed sequentially through a Dowex 50 cation exchange resin column (Sigma), Ambersep 900 quaternary ammonium anion exchange resin (Fluka), Amberlite anion exchange resin (Sigma) and finally a C18 pre-cartridge (Sigma).

Synthesis of Fludeoxyglucose (FGD) Conjugated MNPs

The purified NaF substituted mannose triflate-cysteamine was mixed with the MNPs at room temperature prior to the addition of 50 mM of *N*-Hydroxysuccinimide (Merck) and mixing for 2 hours in an orbital shaker.

Indocyanine Green (ICG) Labelling of FGD-MNPs

7 mg of carbonyl diimidazole (CDI; $\sim$20 mM) and 50 mM of NHS (*N*-Hydroxysuccinimide) were added to 1 mL (30 mg/mL) of FDG-MNPs and mix for 15 minutes at room temperature. The solution was adjusted to a pH of 7.0 using a 2-(*N*-morpholino)ethanesulfonic acid (MES) buffer (0.040 g) and 0.058 g of NaCl and a volume of 2 ml PBS prior to the addition of 0.3 mg/ml of ICG solution (Sigma) and a further 15 minutes mixing at room temperature. Finally, 1.4 μl of mercaptoethanol (20 mM, Sigma) was added to the reaction mixture to inactivate excess ICG and the resulting solution was mixed at room temperature for 2 hours. ICG labelled FDG-MNPs were centrifuged and washed twice with PBS prior to storage in PBS buffer at 4 °C.

Characterization of FDG-MNPs

The size distribution and zeta potential measurements of the ICG labelled FDG-MNPs were performed on a Malvern Zetasizer Nano ZS (Malvern, Herrenberg, Germany) after dilution and sonication of the samples in distilled water. The medium size was 19.43 ± 2.30 nm ($n = 5$) together with their hydrodynamic radius. The particle size and morphology of the ICG labelled FDG-MNPs were assessed by scanning electronic microscopy (Fig. 2(A)) and transmission electron microscopy (Fig. 2(B)). Briefly, samples were freeze-dried

prior to coating with iridium at a thickness of 2 nm (Leica EM ACE600). Samples were examined by scanning electronic microscopy (LEO 1550; Carl Zeiss) with a field-emission electron gun and operation/data acquisition software (Smart SEM version 5). The same samples were also prepared for negative staining with Nano-van (Nanoprobe) and analysed at 120 kV in a transmission electron microscope (JEOL 1400plus) equipped with Gatan Ultrascan 1000 camera. High performance liquid chromatography (HPLC) (Schimadzu, Kyoto, Japan) chromatograms were obtained to check the purity of nanoparticles using a Schimadzu HPLC system equipped with a LC-10ATvp quaternary pump, RF10XL fluorescence detector, and 7.0 μm reversed-phase (RP) -C-18 column (250×21 mm internal diameter) (Macherey-Nagel). ICG labelled FDG-MNPs were checked for excitation and emission spectra at 780 nm 820 nm respectively and eluted in 60% acetonitrile (in distilled water).

In Vivo Analysis of ICG-Labelled FDG-MNP Tissue Distribution

All mice and experimental procedures were conducted using protocols approved by, and in accordance with, the UK Home Office Animal (Scientific Procedures) Act 1986 and the local ethics committee at Aston University. Establishment of sub-cutaneous adenocarcinoma in NMRI mice was conducted as previously described.[38] Briefly, established MAC16 adenocarcinoma were excised from donor NMRI mice and cut into small fragments (approximately 2–5 mm^3) in PBS supplemented with streptomycin and penicillin (Fisher Scientific, UK). Fragments (3–5) were transplanted surgically under isoflurane anaesthesia between the skin and abdominal body-wall of eight, 8-week old NMRI male mice. After 10 days, all mice displayed visible signs of abdominal sub-cutaneous tumour growth. At this time, all mice received ICG-labelled FDG-MNPs at a concentration of 8 mg/kg body weight in 100 μl PBS either intravenously via intravenous injection into the tails vein (4 mice), injection directly into the tumour (3 mice) or injection subcutaneously overlying the tumour (1 mouse). There was no evidence of any ill-effects of ICG-labelled FDG-MNP injection on mouse mobility or general outward behaviour during the experiment. Mice injected intravenously were culled via cervical dislocation at 70 minutes, 2.5 hours, 5 hours or 12 hours post injection, respectively. Similarly, mice receiving injections directly into the tumour were culled at either 70 minutes, 2.5 hours or 5 hours post injection, respectively, while the one mouse injected subcutaneously was culled at 2.5 hours post injection. From all mice, left kidney, liver, lung and tumour were removed and either fixed in 10% neutral buffered formalin (Sigma, UK) for 48 hours at 4 °C, prior to storage in 70% ethanol at 4 °C, or snap frozen and stored at -80 °C.

Tissue RNA Extraction and cDNA Synthesis

Total RNA was extracted from stored kidney, liver, lung and tumour samples using the RNeasy Mini Kit (Qiagen, UK) according to the manufacturer's instructions. Additionally, on column DNase 1 digestion was performed using the RNase-free DNase kit (Qiagen, UK) according to the manufacturer's instructions. RNA was quantified by Nanodrop (ND-1000). cDNA was prepared from 2 μg of RNA using the nanoScript 2 Reverse Transcription kit (Primerdesign, Southampton, UK) with the random primers, according to the manufacturer's instructions. Reverse transcriptase negative (-RT) controls were prepared for all samples as controls for genomic DNA contamination. Synthesised cDNA was diluted in RNase-DNase free water to a concentration equivalent of 5 ng RNA per μl and stored at -20 °C.

Quantitative Real-Time PCR

Intron spanning primers were designed using the Roche Applied Sciences Universal ProbeLibrary Assay Design Centre (See Table I). Gene expression analyses were conducted using the 2X PrecisionPlus Mastermix (Primerdesign) containing SYBR Green, a final concentration of 300 nM each of forward and reverse primers and 1 μl (5 ng RNA equivalent) cDNA in a total volume of 20 μl. Each sample was analysed in triplicate along with respective -RT, no-template (water in place of cDNA) and positive controls. Thermal cycling and fluorescence detection were conducted using a Stratagen Mx3000P qPCR system (Agilent Technologies, Santa Clara, CA, USA) with MxPRO software. Thermal cycling conditions were 95 °C for 2 minutes (enzyme activation), then 40 cycles of 95 °C for 15 seconds followed by 60 °C for 1 minute, with a final

extension step of 70 °C for 1 minute. Melting curves were produced for each sample, measuring fluorescence levels at 0.5 °C intervals.

Tissue Histology and FDG-MNP Distribution

Samples of fixed kidney, liver, lung and tumour from all mice were processed into paraffin wax ahead of sectioning at 5 μm. Tissue sections were analysed either for gross morphology by Haematoxylin and Eosin staining (using standard staining protocols) or for levels of apoptosis using the APO-BrdU TUNNEL Assay Kit (Molecular Probes, Invitrogen, UK) according to the manufacturer's instructions. Haematoxylin and Eosin stained sections were imaged using a CETI Magnum-T microscope connected to a Jenoptik ProgRes CF camera. APO-BrdU TUNNEL stained sections were imaged on a Leica Microstystems DMI 4000B microscope fitted with a Leica DFC360 FX camera. Fluorescent images were captured with filters set for nuclear staining with propidium iodide and for apoptotic nuclei staining with an Alexa Fluor 448 dye-labelled anti BrdU antibody. Relative tissue fluorescent staining intensities were measured from four separate sections of each tissue sample using Volocy software.

Data Analysis

C_t values were converted to relative expression values using the ΔC_t and reference gene stability was calculated using the VBA applet for geNorm.[39] A normalisation factor was derived from the geNorm output which was then used to normalise the expression of each individual gene. See Figure 1 for an outline of the experimental design of this study.

Table I. Real-time qPCR primer details.

Gene name	Gene symbol	Accession number	Primer sequences		Amplicon length
			Forward primer	Reverse primer	
BCL2-associated agonist of cell death	*Bad*	NM_007522.3	gccctaggcttgaggaagtc	catactctgggctgctggtc	90
BCL2-associated X protein	*Bax*	NM_007527.3	agtgtctccggcgaattg	ccacgtcagcaatcatcct	69
B cell leukemia/lymphoma 2	*Bcl2*	NM_009741.5	gtacctgaaccggcatctg	gctgagcagggtcttcagag	130
BCL2-like 1	*Bcl2l1*	NM_001012477	gtcctcttgctgtccagctc	tggtttaccgtcactgatgc	121
Caspase 1	*Casp1*	NM_009807.2	caagtgcaagtgcaaaccag	ggcagcaaattctttcacct	114
Fas (TNF receptor superfamily member 6)	*Fas*	NM_007987.2	acgcttctccgaagactgg	gggttccatgttcacacga	86
Hypoxanthine guanine phosphoribosyl transferase	*Hprt1*	NM_013556.2	tcctcctcagaccgctttt	cctggttcatcatcgctaatc	90
Phosphoglycerate kinase 1	*Pgk1*	NM_008828	tacctgctggctggatgg	cacagcctcggcatatttct	65
Peptidylprolyl isomerase B	*Ppib*	NM_011149	ttcttcataaccacagtcaagacc	accttccgtaccacatccat	92
Succinate dehydrogenase complex, subunit A,	*Sdha*	NM_023281	tgttcagttccaccccaca	tctccacgacacccttctgt	66
TATA box binding protein	*Tbp*	NM_013684.3	gggagaatcatggaccagaa	gatgggaattccaggagtca	90
Tubulin, alpha 1A	*Tuba1*	NM_011653	ctggaacccacggtcatc	gtggccacgagcatagttatt	114

(1) Synthesise FDG-MNPs

(2) Establish tumours in NMRI mice

(3) Inject mice with FDG-MNPs

(4) Analyse tissue morphology

(5) Analyse FDG -MNP distribution
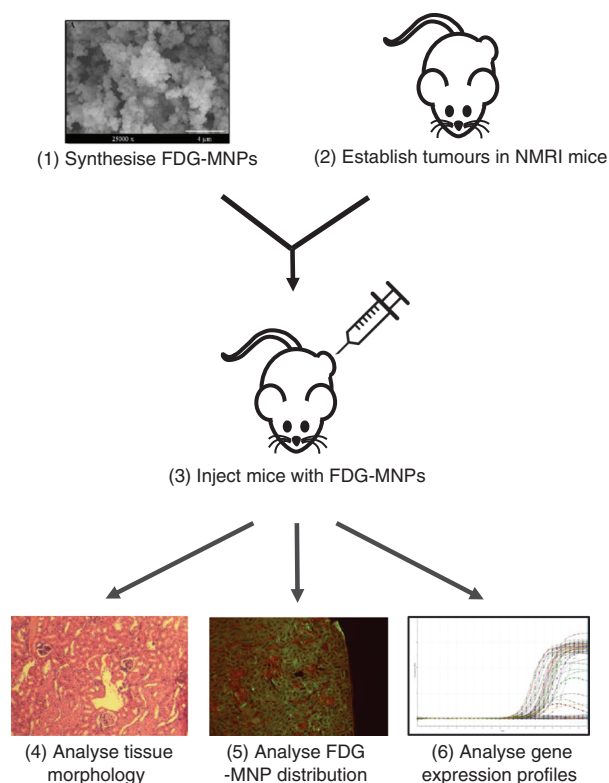
(6) Analyse gene expression profiles

Figure 1. Diagram showing the study experimental design. First, ICG-labelled FDG-MNPs were synthesises and characterised. Second, MAC16 adenocarcinomas were established in male NMRI mice. Mice were injected with ICG-labelled FDG-MNPs (8 mg/kg body) either intravenously, directly into the tumour or subcutaneously directly overlying the tumour. Mice were left for up to 12 hours prior to analysis of tissue morphology, ICG-labelled FDG-MNP tissue distribution and apoptosis pathway gene expression.

RESULTS

Characterisation of ICG-Labelled FDG-MNPs

Reaction yields were calculated as $92.39 \pm 7.4\%$ ($n = 3$) for mannose triflate thiol amide ((3,4,6-tri-O-acetyl-N-(2-mercaptoethyl)-2-O-[(trifluoromethyl)sulfonyl]-d-erythro-hexopyranosylamine-3,4,6-tri-O-acetyl-2-O-[(difluoromethyl) sulfonyl]-d-erythro-hexopyranose (1:1) and 100% ($n = 3$) for the inactive fluorinated derivative of mannose triflate thiol amide (3,4-di-O-acetyl-2-deoxy-2-fluoro-N-(2-mercaptoethyl)hexopyranuronosylamine) according to HPLC chromatograms similar to our previous results.[5, 25] Scanning electron microscopy (SEM) and transmission electron microscopy (TEM) images demonstrated that ICG-labelled FDG-MNP displayed a mean size between 10 to 20 nm. Additionally SEM data showed that the nanoparticles had a cubic spinel structure. The surface potential of the MNPs and FDG-MNPs were found to be -4.77 ± 0.918 mV and 21.26 ± 0.862 mV respectively. Conjugating with FDG resulted in a decrease of negative zeta-potential while also increasing the size of MNPs. HPLC analyses confirmed that synthesized FDG-MNPs

were pure. Synthesized FDG-MNP had an iron oxide concentration of 9.37 mg/mL.

Comparison of Tumour Reference Gene Stability

We observed no detectable impairment in mice well-being or behaviour in response to FDG-MNP injection for up to 12 hours. Previously, we observed a cell death rate of 72% in response to exposure to our FDG-MNPs *in vitro* without magnetic field stimulation.[25] Therefore, in the current study we assessed tissue tumour expression of several genes involved in apoptosis to define the *in vivo* impact of our FDG-MNPS on cell death.

As the accurate measurement of gene expression depends fundamentally on normalisation against stable reference gene(s), we used the geNorm software[39] to define the most stable reference genes within our tumour tissue samples. The geNorm software calculates the average pairwise variation of each reference genes with all the other genes, generating a gene-stability measure (M) for each gene (Fig. 2(A)).[39] Genes with the lowest M value are considered the most stable. Using the geNorm software, systematic exclusion of the least stable genes can be conducted until the remaining two most stable genes are left. However, in this study, we observed substantial variability in most of the reference genes analysed, with four (*Tbp*, *Tuba*, *Hprt* and *Sdha*) out of the six gene having an M value greater than 1 (Fig. 2(B)). However, the two most stable genes were *Ppib* and *Pgk1*.

In addition, geNorm also calculates the optimal number of reference genes needed for any analysis of gene expression, with a value of 0.15 defined as the optimal cut off for appropriate normalisation. Upon reaching this threshold, no further reference genes need be included. In our analyses, only when using four to five reference genes did the stability value drop below 0.15 (Fig. 2(C)), indicating that the most stable four to five reference gene should be used to generate the normalisation factor. To determine the potential impact of using differing numbers of reference genes, we compared the calculated geNorm normalisation factor when using the most stable two, four or all six genes (Fig. 2(D)). Here, we observed that for tissues sampled at 2.5 hours post subcutaneous or direct injection, the number of reference genes used had little impact on the calculated normalisation factor. However, for tissues sampled at 70 minutes post direct injection and 2.5 hours post intra-venous injection, large differences in the calculated normalisation factor was observed depending on the number of reference genes used.

Tumour Gene Expression Profile

We also compared the expression profile of several genes associated with apoptosis using the tumours tissue from mice that had been exposed to ICG-labelled FDG-MNPs. Our goal was to define the impact of MNPs in their non-activated state on tumour tissue. Due to the high level of
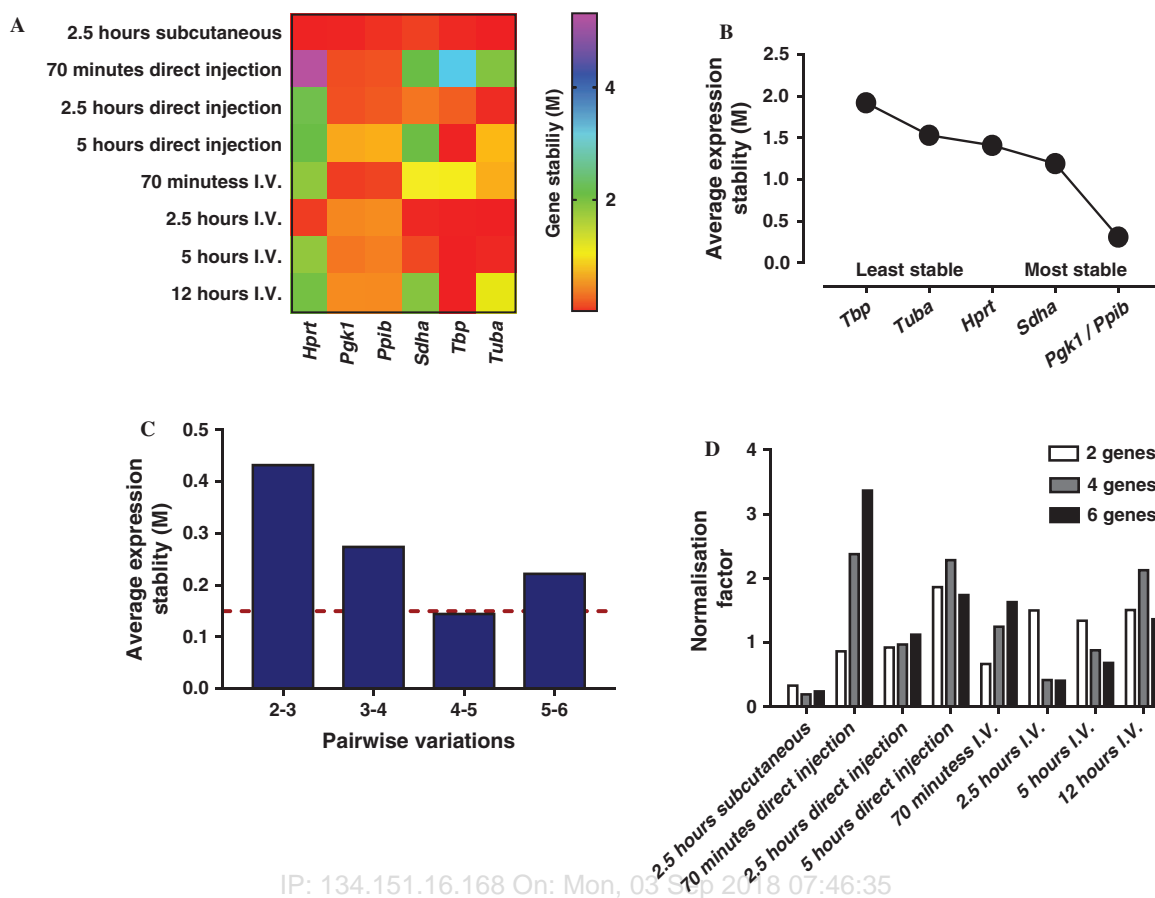
Figure 2. Heat map showing tumour reference gene stability (*M* value), as calculated by geNorm software, for *Hprt*, *Pgk1*, *Ppib*, *Sdha*, *Tbp* and *Tuba* in response to FDG-MNP exposure (A). Mean tumour reference gene stability across all tumour samples (B). Pairwise comparison of gene stability for determination of optimal number of reference genes required for accurate normalisation for genes of interest (C). geNorm generated normalisation factor for each tumour sample showing the effect of using 2, 4 or 6 reference genes (D).

variability in the calculated normalisation factor, depending on how many reference genes were used, we compared gene expression profiles using both the most stable two genes (*Pgk1* and *Ppib*) as well as using all six reference genes.

Similar to the variability observed in reference gene expression, we observed large differences in the expression profiles of our apoptosis genes of interest. For *Bad* (Bcl2-associated agonist of cell death), the highest expression levels were found in tumour tissues at 2.5 hours post subcutaneous injection, 5 hours post direct injection or 12 hours post intra-venous injection (Fig. 3(A)), with *Bad* expression being low in all other tissue samples. We also observed that *Bad* expression profiles were similar irrespective of whether we normalised against two or six reference genes. A similar profile was observed for *Bax* (BCL2-associated X protein), whereby the highest expression was observed in tumour tissue sampled 5 hours post direct tumour injection or 12 hours post intra-venous injection (Fig. 3(B)). For *Bcl2* (suppressor of apoptosis B cell leukemia/lymphoma 2), we observed

comparatively high expression only in tumour tissues collected 2.5 hours post subcutaneous injection of the ICG-labelled FDG-MNPs (Fig. 3(C)), with very low expression detected in all other samples. Comparatively low levels of expression were also observed for *bcl2l1* (BCL2-like 1), also an inhibitor of apoptosis, with some differences in expression profile dependent on the number of references genes used for normalisation (Fig. 3(D)). Similarly, differences between the expression profiles of Caspase 1 (*casp1*) (Fig. 3(E)) and Tumor necrosis factor receptor superfamily member 6 (*Fas*) (Fig. 3(F)) were seen depending on whether two or six references were used for normalisation.

Tissue Morphological Analysis

Histological analysis of kidney, liver, lung and tumour tissue revealed no identifiable differences between ICG-labelled FDG-MNP injection routes or times (Fig. 4). All tissues displayed typical structural organisation with clearly defined kidney glomerular and tubules, radial cords of liver cells, lung alveoli and highly-vascularised tumour
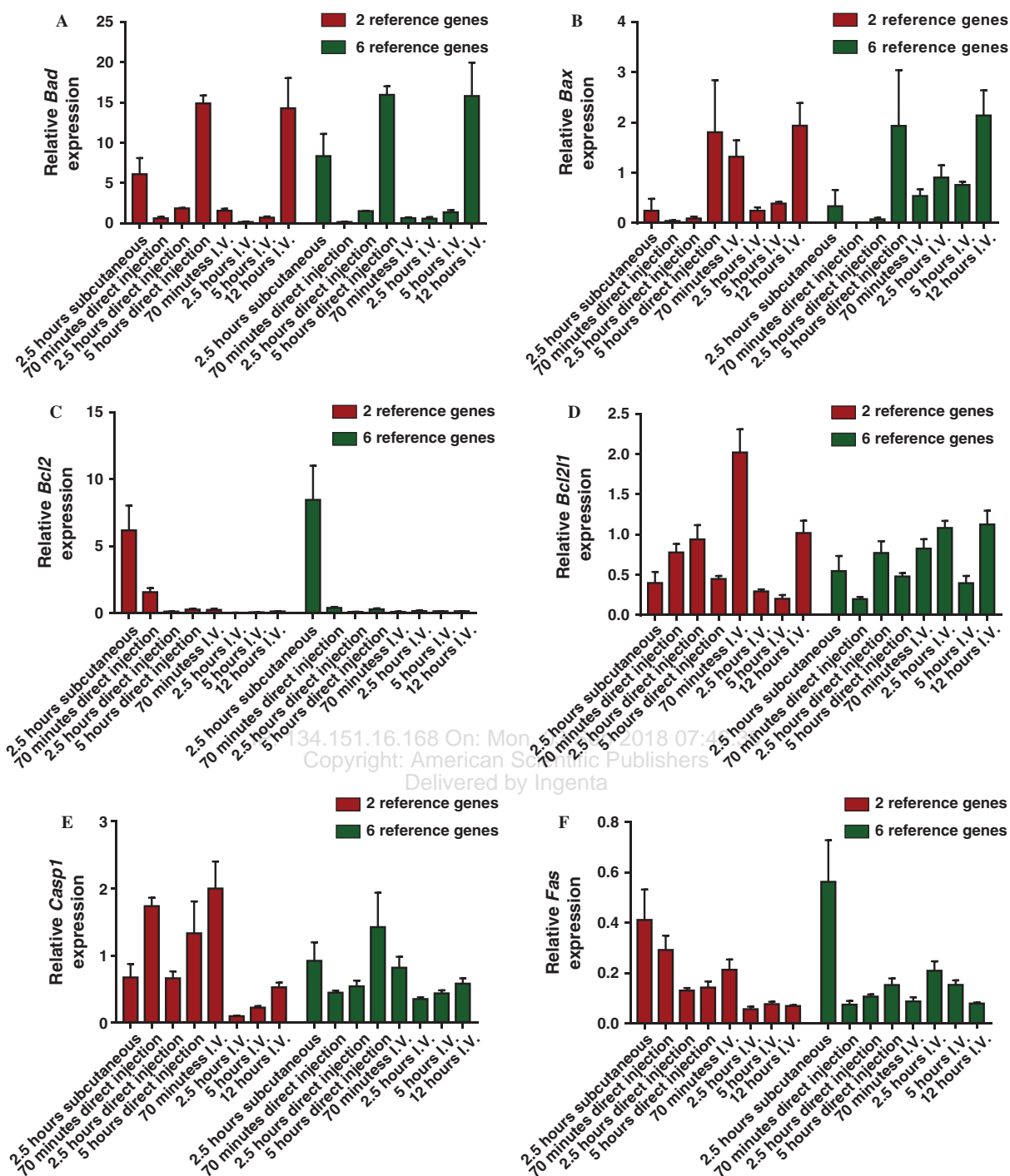
1984

Figure 3. Relative tumour sample expression of apoptosis associated *Bad* (A), *Bax* (B), *Bcl2* (C), *Bcl2l1* (D), *Casp1* (E) and *Fas* (F). Figures display relative expression levels when normalised using the two most stable reference genes (*Pgk1*, *Ppib*) or all 6 reference genes. Values are mean ± S.E.M, $n = 1$ tumour sample per treatment group.

tissues of differing cell morphologies. We observed no significant signs of tissue damage or cellular destruction in any of the tissues examined. These results were supported further by our analysis of apoptosis within the same tissue samples used for gross morphological assessment. We observed no detectable levels of cellular apoptosis, as determined by a lack of nuclear localised signal with

the Alexa Fluor 488 anti-BrdU conjugated antibody. However, we did observe wide distribution of the ICG-labelled FDG-MNP's throughout all of the tissues studied (Fig. 5). In particular we observed diffuse cytoplasmic localisation (e.g., Fig. 5(A), kidney) as well as strong localisation within areas of high vascularity (e.g., Fig. 5(C), tumour).
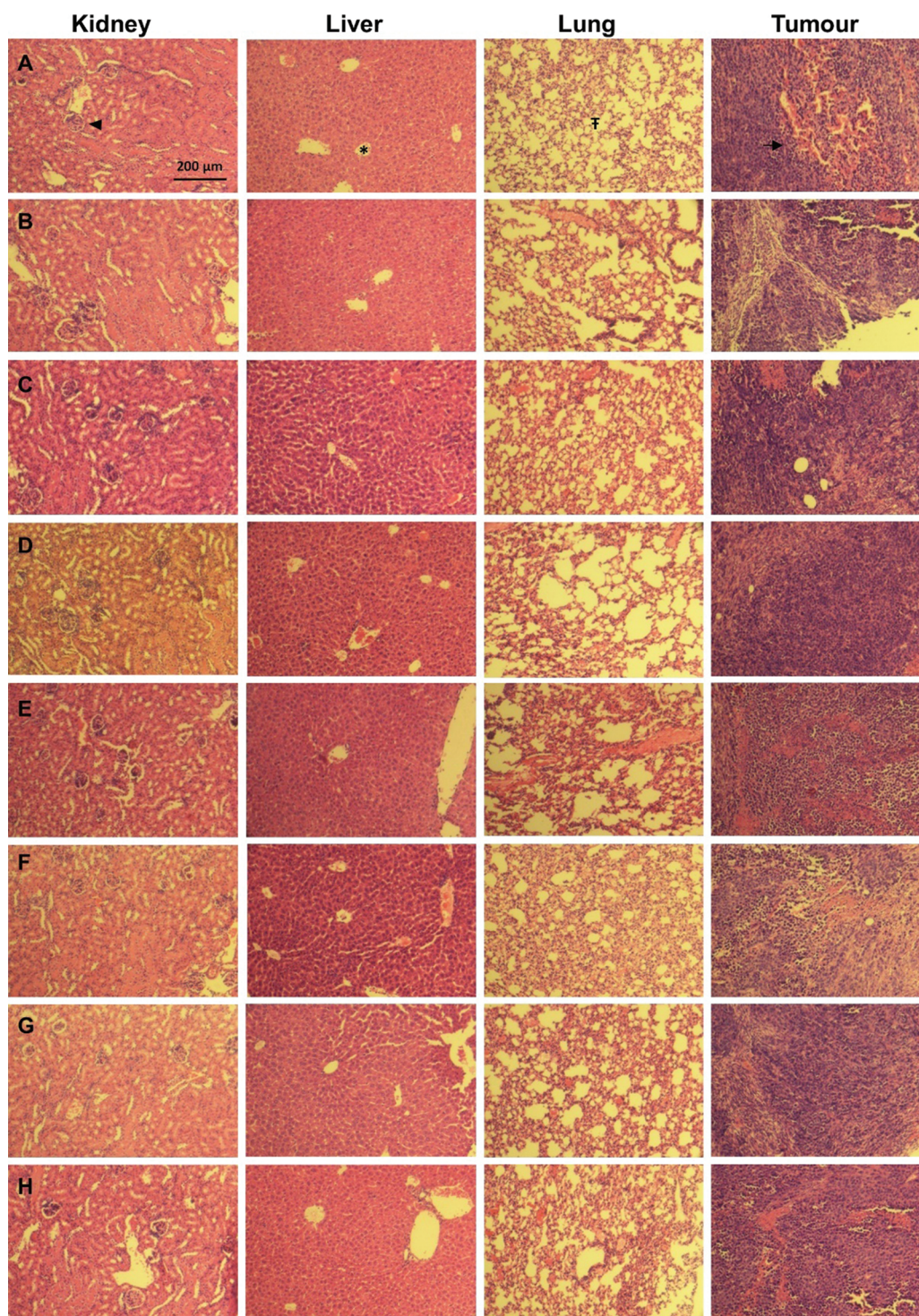
Figure 4. Representative Haemotoxylin and Eosin stained sections from mice injected with ICG-labelled FDG-mNPs at a concentration of 8 mg/kg displaying kidney glomeruli (arrow head), liver central vein (asterisk) and radiating cells, lung alveoli (T) and highly vascularised tumour tissue (arrow). Sections are shown from mice injected either directly into the tumour and analysed after (A) 70, (B) 150 or (C) 300 minutes; intravenously and analysed after (D) 70, (E) 150 or (F) 300 minutes or subcutaneously adjacent to the tumour and analysed after (G) 150 minutes.

Relative Tissue ICG-Labelled FDG-MNP Levels

In kidney tissue, ICG-labelled FDG-MNP signal, normalised to nuclear propidium iodide signal intensity, was highest in tissue samples collected 2.5 hours post subcutaneous injection (Fig. 6(A)). Here, the signal intensity was more than double that of samples collected at 2.5 and 5 hours following either direct or intravenous injection. In all other samples, kidney signal was comparatively similar.
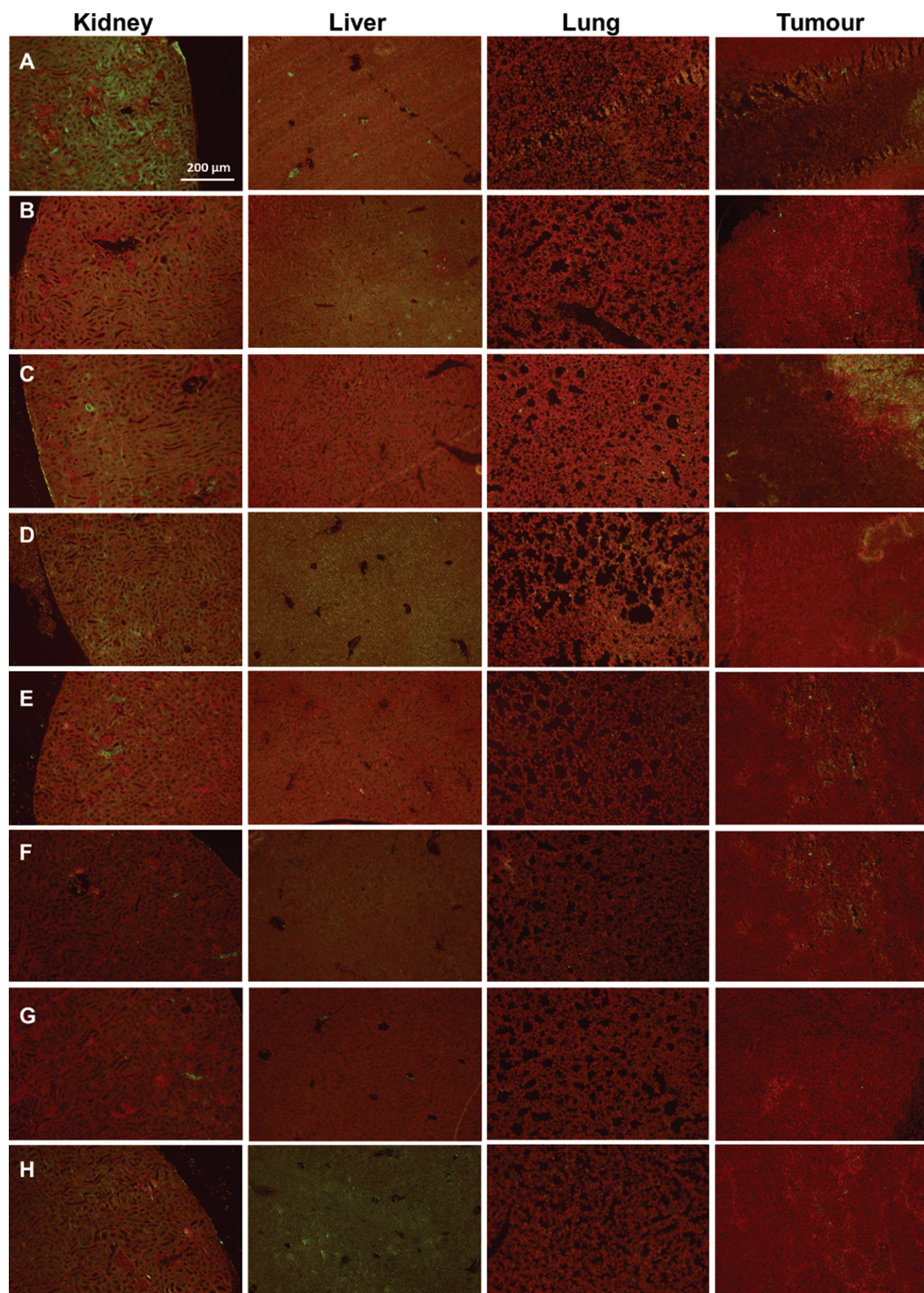
Figure 5. Representative fluorescent images of kidney, liver, lung and tumour tissue sections from mice injected with ICG-labelled FDG-mNPs at a concentration of 8 mg/kg. Sections are stained with propidium iodide to localise nuclei, Alexa fluor 488-conjugated anti-BrdU antibody for apoptotic nuclei. Representative sections are shown from mice injected either directly into the tumour and analysed after (A) 70, (B) 150 or (C) 300 minutes; intravenously and analysed after (D) 70, (E) 150 or (F) 300 minutes or subcutaneously adjacent to the tumour and analysed after (G) 150 minutes.

In liver tissue taken from mice injected intravenously, directly or subcutaneously, minimal changes in tissue signal intensity were observed over time (Fig. 6(B)). However, the highest signal was detected in samples collected at 12 hours post I.V injection (Fig. 6(B)).

Analysis of lung tissue revealed the signal intensity varied little between experimental times and methods of
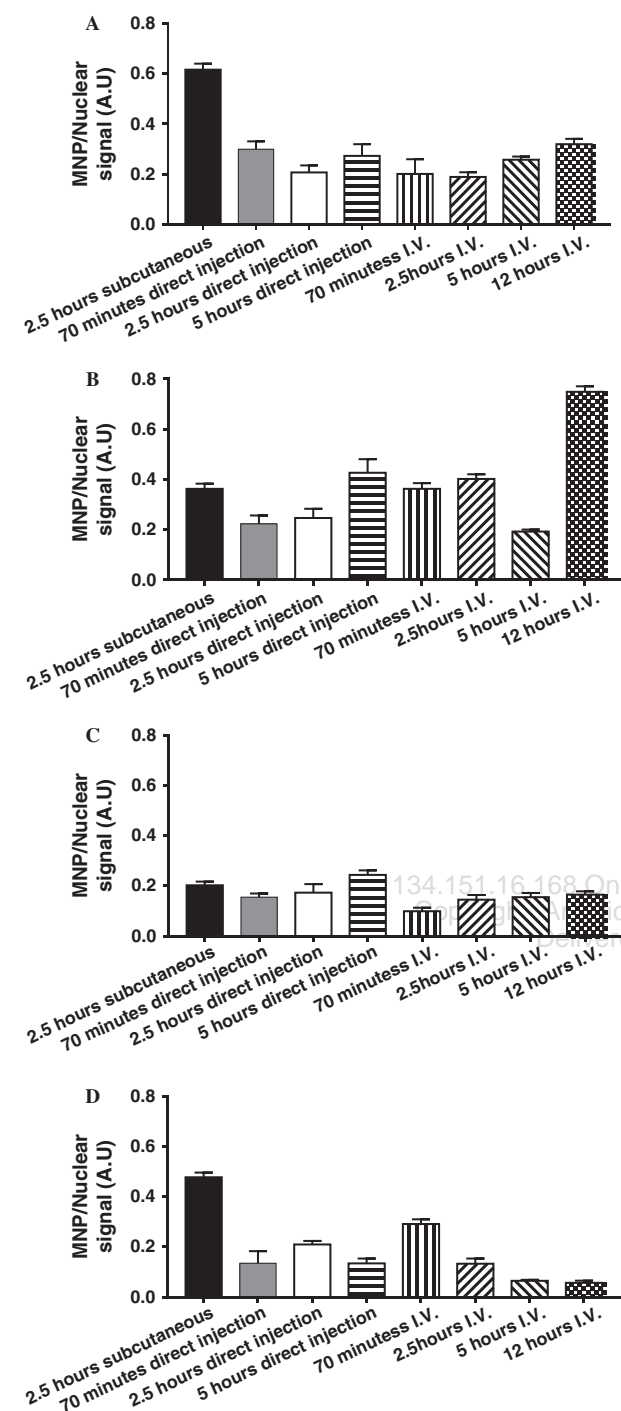
Figure 6. Tissue intensity (arbitrary units) staining for ICG-labelled FDG-mNPs normalised to nuclear propidium iodide signal in (A) kidney, (B) liver, (C) lung and (D) tumour tissues from mice injected either directly into the tumour, intravenously or subcutaneously adjacent to the tumour. Values are mean ± S.E.M of four sections per sample, $n = 1$ mouse per treatment group.

injection (Fig. 6(C)). Finally, analysis of ICG-labelled FDG-MNP signal within the tumour revealed the highest intensity in response to subcutaneously injection, with samples taken 70 minutes following I.V injection having the second highest signal (Fig. 6(D)). For all other samples, minimal differences were observed in ICG-labelled FDG-MNP signal intensities.

DISCUSSION

With current Cancer Research UK estimates that 1 in 2 people born after 1960 in the UK will develop cancer within their lifetime, the development of new approaches to treating cancer has never been more necessary. We have demonstrated previously that FDG-MNPs are actively taken up within MCF-7 cancer cells *in vitro*.[25] Following magnetic field stimulation, we observed that FDG-MNPs led to rapid and sustained cellular hyperthermia, inducing a cell death rate of 89%. However, we also observed a cell death rate of 72% when exposed to the FDG-MNPs when not placed within a magnetic field, suggestive of potential toxicity of the FDG-MNPs. Therefore, in the current study, we determined the *in vivo* impact of FDG-MNPs on tumour and non-tumour tissue without magnetic field heating. We observed highly variable expression of several reference genes used commonly in gene expression analyses studies. As a result, our analysis of tumour tissue apoptosis regulating genes of interest varied depending on the number of reference genes used for normalisation. Secondly, we observed that the duration of exposure and route of FDG-MNP administration led to specific effects on the expression of key regulatory genes such as *Bad*, *Bax*, *Bcl2l1*, *Casp* and *Fas*. Finally, although we observed changes in apoptosis pathway gene expression between treatment groups, we saw no overt gross impact on tissue integrity or levels of apoptosis as determined by histology and TUNNEL staining.

RT-qPCR has become a standard technique for the analysis of cellular and tissue gene expression profiles. However, the validity of any such analyses is dependent on the appropriate selection of reference genes which are suited to the tissue being analysed and that displaying minimal variability between treatment groups. The consequence of using unsuitable and highly variable reference genes is that inaccurate interpretation of expression profiles for the gene of interest may occur. Studies have shown that the use of a single, unstable reference gene alone can affect greatly the expression of a target gene several fold[40, 41] and that differences in expression can be detected when there are none.[40, 42] It is now commonly agreed upon that at least two reference genes should be used for the accurate normalisation of changes in gene expression.[39]

Several software programs are now available for the accurate determination of reference gene stability. In our current study, we used the geNorm package to determine the pairwise variation of six reference genes to each other. We observed that two (*Pgk1* and *Ppib*) of our six reference genes displayed sufficient stability to be considered as suitable reference genes within our study with an *M* value of below 0.15.[39] However, studies have identified these genes

to be either highly variable or differentially expressed in tumour samples.[43, 44] In one study, *PGK1* and *PPIA* (Peptidyl-prolyl cis-trans isomerase A) were undetectable by RNA-Seq in human lung squamous cell carcinoma, and so were deemed inappropriate for use as reference genes.[45] The differences between these observations and ours may be explained by the analogous comparison to the difference between human and mouse samples, as well as the difference between analyses in cell line and primary tissues. Indeed, several studies have shown that the selection of the most appropriate reference gene in cancer tissue is dependent on the specific nature of the experiment.[35–37, 46] Therefore, we suggest that for any study exploring gene expression changes in cancer samples, cell lines or primary tissue, appropriate reference gene identification should be conducted prior to the analysis of target gene expression.

Within our mouse adenocarcinoma model, we also analysed the expression profiles of several genes of interest that can regulate apoptosis using the abovementioned two most stable reference genes, as well as all six reference genes. Apoptosis is the coordinated cellular process of programmed cell death. *Bcl-2* and *Bcl2l1* regulate the main step in the apoptotic pathway, thereby acting as inhibitors of apoptosis.[47] In contrast, *Bad*, *Bax*, *Casp1* and *Fas* act as promotors of apoptosis.[48] We observed that only *Bcl2* displayed high expression levels in samples taken following subcutaneous injection over the tumour. In all other samples, expression was almost undetectable. Expression of *Bcl2l1* was variable across samples, with no specific pattern of expression identified. In contrast, we observed high expression levels of the pro-apoptotic factors *Bad* and *Bax* in tissue sampled at 2.5 hours post subcutaneous injection, 5 hours post direct injection and 12 hours post intravenous injection, irrespective of whether we used two or six reference genes. Finally, *Casp1* and *Fas* displayed similar profiles in that their expression increased over time, whether in samples from tumours injected directly or intravenously. In addition, for *Casp1* and *Fas*, high levels were seen 70 minutes after injection, possibly indicating initial short term responses to the FDG-MNPs. These initial responses would be in agreement with our previous findings in which 72% of cancer cells *in vitro* died in response to being exposed to FDG-MNPs.[25] These results suggest that the expression of the inhibitors of apoptosis (*Bcl2*, *Bcl2l1*) remains relatively stable, while expression of the pro-apoptotic factors varies. Disruption to the normal balance of pro- and anti-apoptotic regulators can result in differential patterns of cell death. Overexpression of *Bcl-2* has been shown to protect prostate cancer cells,[49] and neuroblastoma, glioblastoma and breast carcinoma from apoptosis.[50] In contrast, leukaemogenesis is associated with a reduced level of apoptosis involving increase *Bcl2:Bax* ratios.[51]

Our final observation was that while FDG-MNPs were taken-up readily into all tissues, we observed

no detrimental impact on tissue morphology or levels of apoptosis as determined by TUNNEL staining. In our study, we conjugated our MNPs with the non-metabolisable analogue of glucose FDG. Cancer cells have higher metabolic rates than non-tumour tissue, known as the 'Warburg Effect,'[52] and so have higher levels of glucose uptake and lactate production. Therefore, the preferential uptake of FDG conjugated MNPs into tumour tissue affords us the opportunity to target them specifically for magnetic field-induced hyperthermia. Indeed, recent studies have shown that targeting of MNPs to tumour tissue can be an effective way to dramatically reduce tumour size.[15] We observed no overt sign of tissue damage in response to FDG-MNP administration in histological samples of kidney, liver, lung or tumour tissue. These findings agree with our analysis of apoptosis, as determine by TUNNEL staining. Here we observed no detectable signal for apoptosis in any of our samples. Despite detecting variable expression profiles for several apoptosis pathway genes, our analyses may have been conducted too early, preventing changes detectable at the gene expression level from being translated in changes at the protein or cell function level.

As our FDG-MNPs were labelled also with ICG, we were able to assess their tissue distribution under fluorescence. Here, we detected FDG-MNPs in all tissues as soon as 70 minutes post injection. Interestingly, for all of the tissues, we observed high levels of FDG-MNPs following subcutaneous injection. Also, we observed that the kidney and liver tissue displayed higher levels of FDG-MNPs than the lung or tumour tissues. These findings might reflect the comparatively high metabolic status of these tissues. Finally, we observed also that levels of MNPs were still detectable at 12 hours post-injection. Studies have also demonstrated the non-toxic impact of MNPs on tissue status. Mice treated with silica coated MNPs for 4 weeks show distribution in multiple tissues including the brain, lungs, heart and kidneys, but with no visible toxicity.[53, 54]

We acknowledge that the findings from our current our study require further validation. Future studies will build further on our existing pilot data, involve increased numbers of mice, kept for longer periods of time post FDG-MNP administration and involve more detailed tissue biochemical and molecular analyses. Furthermore, a broader analysis of tissues than those conducted in this study e.g., spleen and heart, would add further insight into the bio-compatibility and physiological impact of our FDG-MNPs. However, our current data indicate the non-toxic impact of FDG-MNPs on tissue and whole body well-being. These findings pave the way for more targeted approached in which we will target FDG-MNP incorporated tumours with focused magnetic fields. Our data offer new approaches for the treatment of cancer which are non-toxic, easily administered and cost-effective and which

will complement existing chemotherapy and radiotherapy approaches.

REFERENCES

1. C. Treanor and M. Donnelly, Late effects of cancer and cancer treatment—The perspective of the patient. *Supportive Care in Cancer: Official Journal of the Multinational Association of Supportive Care in Cancer* 24, 337 (**2016**).

2. Y. A. Luqmani, Mechanisms of drug resistance in cancer chemotherapy. *Medical Principles and Practice: International Journal of the Kuwait University, Health Science Centre* 14(Suppl 1), 35 (**2005**).

3. M. K. Kang and S. K. Kang, Tumorigenesis of chemotherapeutic drug-resistant cancer stem-like cells in brain glioma. *Stem Cells Dev.* 16, 837 (**2007**).

4. G. Vallejo-Fernandez, O. Whear, A. G. Roca, S. Hussain, J. Timmis, V. Patel, and K. O'Grady, Mechanisms of hyperthermia in magnetic nanoparticles. *J. Phys. D Appl. Phys.* 46, Article ID: 312001 (**2013**).

5. F. Ozkaya, P. Unak, E. I. Medine, S. Sakarya, G. Unak, and S. Timur, (18) FDG conjugated magnetic nanoparticle probes: Synthesis and *in vitro* investigations on MCF-7 breast cancer cells. *J. Radioanal. Nucl. Ch.* 295, 1789 (**2013**).

6. J. H. Lee, J. T. Jang, J. S. Choi, S. H. Moon, S. H. Noh, J. W. Kim, J. G. Kim, I. S. Kim, K. I. Park, and J. Cheon, Exchange-coupled magnetic nanoparticles for efficient heat induction. *Nat. Nanotechnol.* 6, 418 (**2011**).

7. L. M. Lacava, Z. G. M. Lacava, R. B. Azevedo, S. B. Chaves, V. A. P. Garcia, O. Silva, F. Pelegrini, N. Buske, C. Gansau, M. F. Da Silva, and P. C. Morais, Use of magnetic resonance to study biodistribution of dextran-coated magnetic fluid intravenously administered in mice. *J. Magn. Magn. Mater.* 252, 367 (**2002**).

8. N. Kohler, C. Sun, A. Fichtenholtz, J. Gunn, C. Fang, and M. Zhang, Methotrexate-immobilized poly(ethylene glycol) magnetic nanoparticles for MR imaging and drug delivery. *Small* 2, 785 (**2006**).

9. H. Y. Park, M. J. Schadt, L. Wang, Lim II, P. N. Njoki, S. H. Kim, M. Y. Jang, J. Luo, and C. J. Zhong, Fabrication of magnetic core@shell Fe oxide@Au nanoparticles for interfacial bioactivity and bio-separation. *Langmuir* 23, 9050 (**2007**).

10. J. Xie, C. Xu, Z. Xu, Y. Hou, K. L. Young, S. Wang, N. Pourmond, and S. Sun, Linking hydrophilic macromolecules to monodisperse magnetite $(Fe_{(3)}O_{(4)})$ nanoparticles via trichloro-s-triazine. *Chemistry of Materials: A Publication of the American Chemical Society* 18, 5401 (**2006**).

11. X. H. Duan, Y. Wang, F. Zhang, L. J. Lu, M. H. Cao, B. L. Lin, X. Zhang, J. J. Mao, X. T. Shuai, and J. Shen, Superparamagnetic iron oxide-loaded cationic polymersomes for cellular MR imaging of therapeutic stem cells in stroke. *J. Biomed. Nanotechnol.* 12, 2112 (**2016**).

12. M. D. Glasgow and M. B. Chougule, Recent developments in active tumor targeted multifunctional nanoparticles for combination chemotherapy in cancer treatment and imaging. *J. Biomed. Nanotechnol.* 11, 1859 (**2015**).

13. L. Li, W. Jiang, K. Luo, H. Song, F. Lan, Y. Wu, and Z. Gu, Superparamagnetic iron oxide nanoparticles as MRI contrast agents for non-invasive stem cell labeling and tracking. *Theranostics* 3, 595 (**2013**).

14. A. G. Roca, R. Costo, A. F. Rebolledo, S. Veintemillas-Verdaguer, P. Tartaj, T. Gonzalez-Carreno, M. P. Morales, and C. J. Serna, Progress in the preparation of magnetic nanoparticles for applications in biomedicine. *J. Phys. D Appl. Phys.* 42, Article ID: 224002 (**2009**).

15. H. S. Huang and J. F. Hainfeld, Intravenous magnetic nanoparticle cancer hyperthermia. *Int. J. Nanomed.* 8, 2521 (**2013**).

16. C. C. Berry, Progress in functionalization of magnetic nanoparticles for applications in biomedicine. *J. Phys. D Appl. Phys.* 42, Article ID: 224003 (**2009**).

17. E. Amstad and E. Reimhult, Nanoparticle actuated hollow drug delivery vehicles. *Nanomedicine-Uk* 7, 145 (**2012**).

18. Y. Zhai, H. Xie, and H. Gu, Effects of hyperthermia with dextran magnetic fluid on the growth of grafted H22 tumor in mice. *International Journal of Hyperthermia: The Official Journal of European Society for Hyperthermic Oncology* 25, 65 (**2009**).

19. Y. Shido, Y. Nishida, Y. Suzuki, T. Kobayashi, and N. Ishiguro, Targeted hyperthermia using magnetite cationic liposomes and an alternating magnetic field in a mouse osteosarcoma model. *The Journal of Bone and Joint Surgery* 92, 580 (**2010**).

20. C. L. Dennis, A. J. Jackson, J. A. Borchers, P. J. Hoopes, R. Strawbridge, A. R. Foreman, J. van Lierop, C. Gruttner, and R. Ivkov, Nearly complete regression of tumors via collective behavior of magnetic nanoparticles in hyperthermia. *Nanotechnology* 20, 395103 (**2009**).

21. M. T. Basel, S. Balivada, H. Wang, T. B. Shrestha, G. M. Seo, M. Pyle, G. Abayaweera, R. Dani, O. B. Koper, M. Tamura, V. Chikan, S. H. Bossmann, and D. L. Troyer, Cell-delivered magnetic nanoparticles caused hyperthermia-mediated increased survival in a murine pancreatic cancer model. *Int. J. Nanomedicine* 7, 297 (**2012**).

22. G. Kroemer and J. Pouyssegur, Tumor cell metabolism: Cancer's achilles' heel. *Cancer Cell* 13, 472 (**2008**).

23. E. Racker, Bioenergetics and the problem of tumor growth. *American Scientist* 60, 56 (**1972**).

24. I. San-Millan and G. A. Brooks, Reexamining cancer metabolism: Lactate production for carcinogenesis could be the purpose and explanation of the warburg effect. *Carcinogenesis* 38, 119 (**2016**).

25. M. Subramanian, G. Pearce, O. K. Guldu, V. Tekin, A. Miaskowski, O. Aras, and P. Unak, A pilot study into the use of FDG-mNP as an alternative approach in neuroblastoma cell hyperthermia. *IEEE T Nanobiosci.* 15, 517 (**2016**).

26. E. S. Lucas, A. J. Watkins, A. L. Cox, S. J. Marfy-Smith, N. Smyth, and T. P. Fleming, Tissue-specific selection of reference genes is required for expression studies in the mouse model of maternal protein undernutrition. *Theriogenology* 76, 558 (**2011**).

27. A. Stahlberg, M. Bengtsson, M. Hemberg, and H. Semb, Quantitative transcription factor analysis of undifferentiated single human embryonic stem cells. *Clin. Chem.* 55, 2162 (**2009**).

28. S. A. Bustin, V. Benes, J. A. Garson, J. Hellemans, J. Huggett, M. Kubista, R. Mueller, T. Nolan, M. W. Pfaffl, G. L. Shipley, J. Vandesompele, and C. T. Wittwer, The MIQE guidelines: Minimum information for publication of quantitative real-time PCR experiments. *Clin. Chem.* 55, 611 (**2009**).

29. S. Guénin, M. Mauriat, J. Pelloux, O. Van Wuytswinkel, C. Bellini, and L. Gutierrez, Normalization of qRT-PCR data: The necessity of adopting a systematic, experimental conditions-specific, validation of references. *J. Exp. Bot.* 60, 487 (**2009**).

30. E. Boda, A. Pini, E. Hoxha, R. Parolisi, and F. Tempia, Selection of reference genes for quantitative real-time RT-PCR studies in mouse brain. *J. Molecular Neuroscience* 37, 238 (**2009**).

31. N. Tanic, M. Perovic, A. Mladenovic, S. Ruzdijic, and S. Kanazir, Effects of aging, dietary restriction and glucocorticoid treatment on housekeeping gene expression in rat cortex and hippocampus-evaluation by real time RT-PCR. *J. Molecular Neuroscience* 32, 38 (**2007**).

32. N. A. Janovick-Guretzky, H. M. Dann, D. B. Carlson, M. R. Murphy, J. J. Loor, and J. K. Drackley, Housekeeping gene expression in bovine liver is affected by physiological state, feed intake, and dietary treatment. *J. Dairy Sci.* 90, 2246 (**2007**).

33. K. Goossens, M. Van Poucke, A. Van Soom, J. Vandesompele, A. Van Zeveren, and L. J. Peelman, Selection of reference genes for quantitative real-time PCR in bovine preimplantation embryos. *BMC Dev. Biol.* 5, 27 (**2005**).

34. S. Mamo, A. B. Gal, S. Bodo, and A. Dinnyes, Quantitative evaluation and selection of reference genes in mouse oocytes and embryos cultured *in vivo* and *in vitro*. *BMC Dev. Biol.* 7, 14 (**2007**).

35. L. Lima, C. Gaiteiro, A. Peixoto, J. Soares, M. Neves, L. L. Santos, and J. A. Ferreira, Reference genes for addressing gene expression of bladder cancer cell models under hypoxia: A step towards transcriptomic studies. *PloS One* 11, e0166120 (**2016**).

36. J. L. Martin, Validation of reference genes for oral cancer detection panels in a prospective blinded cohort. *PloS One* 11, e0158462 (**2016**).

37. Y. Niu, Y. Wu, J. Huang, Q. Li, K. Kang, J. Qu, F. Li, and D. Gou, Identification of reference genes for circulating microRNA analysis in colorectal cancer. *Scientific Reports* 6, 35611 (**2016**).

38. M. C. Bibby, J. A. Double, S. A. Ali, K. C. Fearon, R. A. Brennan, and M. J. Tisdale, Characterization of a transplantable adenocarcinoma of the mouse colon producing cachexia in recipient animals. *Journal of the National Cancer Institute* 78, 539 (**1987**).

39. J. Vandesompele, K. De Preter, F. Pattyn, B. Poppe, N. Van Roy, A. De Paepe, and F. Speleman, Accurate normalization of real-time quantitative RT-PCR data by geometric averaging of multiple internal control genes. *Genome Biol.* 183, RESEARCH0034 (**2002**).

40. R. Kosir, J. Acimovic, M. Golicnik, M. Perse, G. Majdic, M. Fink, and D. Rozman, Determination of reference genes for circadian studies in different tissues and mouse strains. *BMC Molecular Biology* 11, 60 (**2010**).

41. A. P. Piehler, R. M. Grimholt, R. Ovstebo, and J. P. Berg, Gene expression results in lipopolysaccharide-stimulated monocytes depend significantly on the choice of reference genes. *BMC Immunology* 11, 21 (**2010**).

42. J. A. van den Bergen, D. C. Miles, A. H. Sinclair, and P. S. Western, Normalizing gene expression levels in mouse fetal germ cells. *Biology of Reproduction* 81, 362 (**2009**).

43. M. Krzystek-Korpacka, K. Hotowy, E. Czapinska, M. Podkowik, J. Bania, A. Gamian, and I. Bednarz-Misa, Serum availability affects expression of common house-keeping genes in colon adenocarcinoma cell lines: Implications for quantitative real-time PCR studies. *Cytotechnology* 68, 2503 (**2016**).

44. Y. Midorikawa, S. Tsutsumi, H. Taniguchi, M. Ishii, Y. Kobune, T. Kodama, M. Makuuchi, and H. Aburatani, Identification of genes associated with dedifferentiation of hepatocellular carcinoma with expression profiling analysis. *Japanese Journal of Cancer Research* 93, 636 (**2002**).

45. C. Zhan, Y. Zhang, J. Ma, L. Wang, W. Jiang, Y. Shi, and Q. Wang, Identification of reference genes for qRT-PCR in human lung squamous-cell carcinoma by RNA-Seq. *Acta Biochimica et Biophysica Sinica* 46, 330 (**2014**).

46. L. Y. Fu, H. L. Jia, Q. Z. Dong, J. C. Wu, Y. Zhao, H. J. Zhou, N. Ren, Q. H. Ye, and L. X. Qin, Suitable reference genes for real-time PCR in human HBV-related hepatocellular carcinoma with different clinical prognoses. *BMC Cancer* 9, 49 (**2009**).

47. S. Cory and J. M. Adams, The Bcl2 family: Regulators of the cellular life-or-death switch. *Nature Rev. Cancer* 2, 647 (**2002**).

48. R. S. Wong, Apoptosis in cancer: From pathogenesis to treatment. *J. Experimental and Clinical Cancer Research* 30, 87 (**2011**).

49. A. J. Raffo, H. Perlman, M. W. Chen, M. L. Day, J. S. Streitman, and R. Buttyan, Overexpression of bcl-2 protects prostate cancer cells from apoptosis *in vitro* and confers resistance to androgen depletion *in vivo*. *Cancer Research* 55, 4438 (**1995**).

50. S. Fulda, E. Meyer, and K. M. Debatin, Inhibition of TRAIL-induced apoptosis by Bcl-2 overexpression. *Oncogene* 21, 2283 (**2002**).

51. C. Goolsby, M. Paniagua, M. Tallman, and R. B. Gartenhaus, Bcl-2 regulatory pathway is functional in chronic lymphocytic leukemia. *Cytometry, Part B, Clinical Cytometry* 63, 36 (**2005**).

52. M. V. Liberti and J. W. Locasale, The warburg effect: How does it benefit cancer cells? *Trends in Biochemical Sciences* 41, 211 (**2016**).

53. J. S. Kim, T. J. Yoon, K. N. Yu, B. G. Kim, S. J. Park, H. W. Kim, K. H. Lee, S. B. Park, J. K. Lee, and M. H. Cho, Toxicity and tissue distribution of magnetic nanoparticles in mice. *Toxicol Sci.* 89, 338 (**2006**).

54. J. T. Kwon, S. K. Hwang, H. Jin, D. S. Kim, A. Minai-Tehrani, H. J. Yoon, M. Choi, T. J. Yoon, D. Y. Han, Y. W. Kang, B. I. Yoon, J. K. Lee, and M. H. Cho, Body distribution of inhaled fluorescent magnetic nanoparticles in the mice. *J. Occupational Health* 50, 1 (**2008**).